

OHAM Analysis of Bio-Convective Flow of Oldroyd-B nanofluid under Thermal Radiation Impact Past over a Stretching Sheet

Muhammad Sohail¹*, Komal Ilyas¹, Esha Rafique¹, and Shah Jahan¹

¹Institute of Mathematics, Khwaja Fareed University of Engineering & Information Technology, Rahim Yar Khan 64200, Pakistan

Corresponding Author: muhammad_sohail111@yahoo.com;

Mobile number: +92 300 5345466

Abstract: In this work, we examine the Heimburg model, which describes how electromechanical pulses are transmitted through nerves by using the generalizing Riccati equation mapping method. This approach is regarded as one of the most recent efficient analytical approaches for nonlinear evolution equations, yielding numerous different types of solutions for the model under consideration. We get novel analytic exact solitary wave solutions, including exponential, hyperbolic, and trigonometric functions. These solutions comprises solitary wave, kink, singular kink, periodic, singular soliton, combined dark bright soliton, and breather soliton. To understand the physical principles and significance of the technique the well-furnished results are ultimately displayed in a variety of 2D, 3D, and contour profiles. Furthermore, this system's linearized stability is examined. The results of this work shed light on the importance of studying various nonlinear wave phenomena in nonlinear optics and physics by showing how important it is to understand the behaviour and physical meaning of the studied model. The employed methodology possesses sufficient capability, efficacy, and brevity to enable further research.

Keywords: Oldroyd-B nanofluid; Thermal Radiation; MHD; Thermophoresis effect; OHAM; Heat generation.

1. Introduction

Oldroyd-B nanofluids are used in medication delivery and improved heat transfer systems, and precise material handling because of their distinct rheological characteristics. Applications of bioconvection are found in medical study, monitoring the surroundings and enhancing the movement of fluids in pharmaceutical and biotechnology operations. Liquid solutions containing nanoparticles are known as nanofluids, improving fluid characteristics and heat transmission, with uses in materials science, electronics, and clinical. Oldroyd-B nanofluids are utilized in innovative cooling systems to improve thermal performance for electronic devices and power plants. They can also be used in heat exchangers to improve energy efficiency in industrial procedures. Nanofluids Oldroyd-B converge non-Newtonian Oldroyd-B fluid model featuring particles at nanoscale, influencing rheology for possible uses in various domains [1-4]. The Oldroyd-B nanoparticles' blood flow, with the heat radiation and heat transfer properties brought on by constricted arteries.

In the numerical investigation, Jawad et al. [5] delved the flow of an Oldroyd-B nanofluid through a stretched sheet in a boundary layer involving heat transmission. Heat transfers as well as convective flow in a viscous nanofluid were explored by Romila et al. [6]. The effects of a thermally transmitted non-Newtonian nanofluid among an infinite pipe have been studied by Ellahi [7]. In bi-engineering, Khan and Ali [8] emphasized the significance of bioconvection by outlining the analysis for Eyring-Powell nanofluid's erratic transport and the importance of different temperature characteristics. Chu et al. [9] considered the phenomenon of heat generation and the bidirectionally accelerated flow from the surface of Maxwell nanofluid in conjunction with gyrotactic microorganisms. The addition of the slip process in the Oldroyd-B tiny material in the occurrence of motile microorganisms was asserted by Khan et al. [10]. Ramzan et al. [11] showed the chemical reactive study of the radiative flow of polarized nanofluid with the subsequent contribution of microorganisms. Multiple slip inscriptions in the bioconvection flow of crossed nanofluid beyond moving wedge was illustrated by Alshomrani et al. [12]. The thermal effectiveness of ferromagnetic nanoparticles containing magnetic dipole and a microorganism was assessed by Nadeem et al. [13]. To prove that Carreau nanofluid has thermal uses, Elayarani et al. [14] investigated the bioconvection method. Shehzad et al. [15] investigated the important phenomena of bioconvection among micropolar nanofluids using the modified flux relations. Khan et al. [16] discuss the uses of radiative dynamics to examine the characteristics of bioconvection in the flow of micropolar nanoparticles contained by a revolving disk.

Kuznetsov [17] offered some fantastic applications in addition to an intriguing contribution to the bioconvection flow of nanofluid. The study conducted by Waqas et al. [18] concentrated on the numerical analysis of bioconvection in enhanced second-grade nanofluid. The Oldroyd-B nanofluid's efficient Prandtl method in the existence of microorganisms held within an accelerating surface has been examined analytically by Khan et al. [19].

Irfan et al. [20] looked into how thermal-solutal stratifications affected the OBF stream. The OBF flow model was explored by Alzahrani et al. [21] using heat generation through a cone. Almakki et al. [22] examined entropy formation using the OBF model through thermophoresis and Brownian diffusions. Ramzan et al. [23] illustrated the dipole effect on the OBF stream with freezing and energy activation effects. In their study of heat transmission, Sarada et al. [24] took into account how LTNE affected OBF flow on a sheet. Khan et al. [25] found the radiative flow of an Oldroyd-B fluid in three dimensions via mixed convection across a bidirectional extending surface. Oldroyd-B fluid's three-dimensional flow with the influence of Newtonian heating via a stretched sheet was calculated by Ramzan et al. [26]. Ashraf et al. [27] examined the impact of an Oldroyd-B fluid mixed convection flow along thermal radiation on a wedge surface. By modeling the physical phenomenon with the idea of fractional calculus, Sohail et al. [28] calculated a precise answer for the MHD flow rate of an Oldroyd-B fluid. The impact of a magnetic field on the flow of Oldroyd-B nano-liquid over a stretching sheet was investigated by Sandeep et al. [29]. In stretchable flow of Oldroyd-B liquid, Hayat et al. [30,31] report on the characteristics of temperature-dependent conductivity. Magesh et al. [32] evaluated the effect of the produced magnetic field for the Jeffrey fluid during peristalsis by using curving channel. Magesh et al. [33] developed the impact of activated energy at the peristaltic circulation of a Carreau nanoliquid within a curving asymmetric channel under the significance of a magnetic field. Magesh et al. [34] studied the electro-kinetic peristaltic transportation of a Sutterby tinyfluid in relation to Bejan quantity and entropy formation. They took into account Sutterby nanoliquid motion in the transverse manner under an imposed externally magnetic field and in a horizontal plane under an unvarying electric field. Magesh et al. [35] analyzed the peristaltic behaviour of a Johnson-Segalman tinyfluid over an asymmetric flexible a tiny channel according to the influence of activating energy. Praveen Kumar et al. [36] explored the electrokinetic peristaltic stream of the Sutterby tinyfluid via an asymmetric microconduit having a permeable media and the Joule burning variable. Akbar et al. [37] examined the thermal and motion features of combined convection peristaltic circulation of tinyfluids that contained magnetic γAl_2O_3 tinyparticles dispersed in traditional

liquids, such as water H_2O and ethylene glycol $C_2H_6O_2$. Kezzar et al. [38] evaluated the influence of tertiary hybrid nanoliquid and velocity slippage on the non-Newtonian liquid circulation among two nonparallel panels. Using a mathematical representation of Cross fluids, Ayub et al. [39] inspected the thermal distribution study of trihybrid tiny fluid (blood) through wedge-like arteries. Ayub et al. [40] researched an inclined magnetised Cross fluid circulation incorporated in a complicated chemical procedure with fuzzy circumstances. Hussain Shah et al. [41] explored the simultaneous impacts of shear force, heterogeneous-homogeneous chemical reactions, and convection on the transport behaviour of a tertiary hybrid Carreau bio-nanofluid travelling via a stenosed artery. Using a 3-dimensional Carreau tinyfluid structure across a wedge, Alqudah et al. [42] inspected the modelling of heat transport of a triple magnetised hybrid nanofluid $[(Al_2O_3, CuO, TiO_2)/H_2O]$. A notable involvement was made by Shamshuddin et al. [43] with their thorough analysis of the matter transmission and thermal transfer processes in the $NF ND - Cu/H_2O$ when a continuously expanding velocity was applied. Shamshuddin et al. [44] addressed the bioconvective therapy of the reactionary Casson hybrid nanoliquid circulation via a gradually stretched surface using mixed convection and ohmic warming. Lone et al. [45] explored the Casson hybrid nanofluid stream on an increasingly expanding strip under the influence of gyrotactic microbes. The evaluation of thermally radiative fluctuation and heat in a micropolar nanofluid experiencing stagnant spot circulation was provided by Gamar et al. [46]. The study examines the thermal behavior of the nanofluid in detail, paying particular attention to how pertinent parameters affect the dispersion of energy.

The study makes an important advance to our analyzing of bioconvection in a Darcy-Forchheimer by including shifting thermophysical properties into the Oldroyd-B nanofluid. The study broadens the usual modeling model to account for more likely scenarios by include variables such as Brownian motion, MHD, heat generation, and thermophoresis. This integration improves our understanding of bioconvection dynamics, particularly in complex environments such as porous media with flow resistance and inertial impacts. They applied the homotopy analysis technique to the governing system of problems, which is a highly successful and commonly employed analytical approach for solving highly nonlinear governing equations with linear-related operators and base functions. The outcomes are graphed, and the Nusselt values are presented in tables.

2. Mathematical Model

The study of magnetohydrodynamic (MHD) flow with the effects of mixed convection for a

viscoelastic Oldroyd-B nanofluid in a steady, two-dimensional setup contained in nanoparticles is supervised by a stretched sheet that carries Brownian motion and thermophoresis. Gyrotactic microorganisms are dispersed using water as a base fluid. The Darcy-Forchheimer law is applied to porous media, with the magnetic field aligned along the y -axis. The coordinate system is set such that the x -axis represents the stretching direction, while the y -axis is perpendicular to the stretched sheet (see Fig. 1). The mathematical equations are stated as.

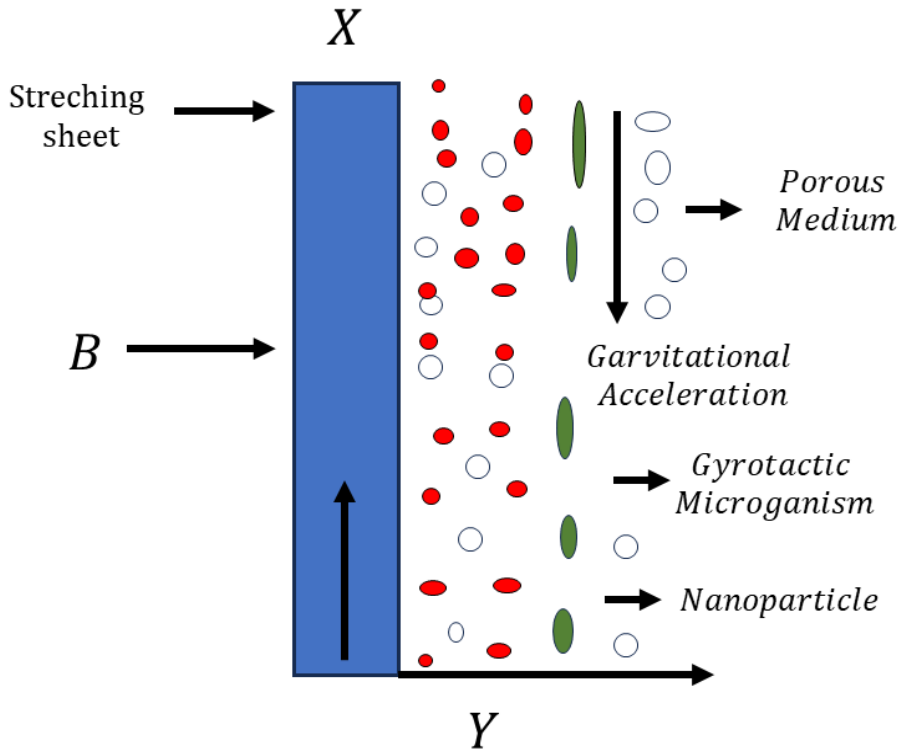


Fig. 1. Flow Geometry.

The problem equations are as follow [50, 51,52,53]:

$$\frac{\partial \bar{u}}{\partial x} + \frac{\partial \bar{v}}{\partial y} = 0, \quad (1)$$

$$\bar{u} \frac{\partial \bar{u}}{\partial x} + \bar{v} \frac{\partial \bar{u}}{\partial y} = -\frac{1}{\rho_f} \frac{\partial p}{\partial x} - \lambda_1 \left(\bar{u}^2 \frac{\partial^2 \bar{u}}{\partial x^2} + \bar{v}^2 \frac{\partial^2 \bar{u}}{\partial y^2} + 2\bar{u}\bar{v} \frac{\partial^2 \bar{u}}{\partial x \partial y} \right)$$

$$+\bar{v} \left(\frac{\partial^2 \bar{u}}{\partial y^2} + \lambda_2 \left(\bar{u} \frac{\partial^3 \bar{u}}{\partial x \partial y^2} + \bar{v} \frac{\partial^3 \bar{u}}{\partial y^3} - \frac{\partial \bar{u}}{\partial x} \frac{\partial^2 \bar{u}}{\partial y^2} - \frac{\partial \bar{u}}{\partial y} \frac{\partial^2 \bar{u}}{\partial y^2} \right) \right) - \frac{\sigma B_0^2}{\rho_f} \bar{u} - \left(\frac{\bar{v}}{K_1} \bar{u} + \frac{Cb}{x\sqrt{K_1}} \bar{u} \right) \bar{u}, \quad (2)$$

$$\bar{u} \frac{\partial \bar{T}}{\partial x} + \bar{v} \frac{\partial \bar{T}}{\partial y} = \alpha \left(\frac{\partial^2 \bar{T}}{\partial x^2} + \frac{\partial^2 \bar{T}}{\partial y^2} \right) - \frac{1}{(\rho c_p)_f} \frac{\partial q_r}{\partial y} + \tau \left[D_B \left(\frac{\partial \bar{C}}{\partial x} \frac{\partial \bar{T}}{\partial x} + \frac{\partial \bar{C}}{\partial y} \frac{\partial \bar{T}}{\partial y} \right) + \frac{D_T}{\bar{T}_\infty} \left(\left(\frac{\partial \bar{T}}{\partial x} \right)^2 + \left(\frac{\partial \bar{C}}{\partial y} \right)^2 \right) \right] - \frac{Q_0}{\rho C_p} (\bar{T} - \bar{T}_\infty), \quad (3)$$

$$\bar{u} \frac{\partial \bar{C}}{\partial x} + \bar{v} \frac{\partial \bar{C}}{\partial y} = D_B \left(\frac{\partial^2 \bar{C}}{\partial x^2} + \frac{\partial^2 \bar{C}}{\partial y^2} \right) + \frac{D_T}{\bar{T}_\infty} \left(\frac{\partial^2 \bar{T}}{\partial x^2} + \frac{\partial^2 \bar{T}}{\partial y^2} \right), \quad (4)$$

$$\bar{u} \frac{\partial \bar{N}}{\partial x} + \bar{v} \frac{\partial \bar{N}}{\partial y} + \frac{bW_c}{(\bar{C}_w - \bar{C}_\infty)} \left[\frac{\partial}{\partial y} \left(\bar{N} \frac{\partial \bar{C}}{\partial y} \right) \right] = D_M \left(\frac{\partial^2 \bar{N}}{\partial y^2} \right). \quad (5)$$

The subjected boundary conditions are [53, 54, 55, 56, 57]:

$$\begin{aligned} \bar{u} = U_w = bx, \bar{v} = 0, \bar{T} = \bar{T}_w, \bar{N} = \bar{N}_w, \bar{C} = \bar{C}_w \text{ at } y = 0, \\ \bar{u} \rightarrow 0, \bar{T} \rightarrow \bar{T}_\infty, \bar{N} \rightarrow \bar{N}_\infty, \bar{C} \rightarrow \bar{C}_\infty \text{ as } y \rightarrow \infty. \end{aligned} \quad (6)$$

Utilizing the renowned Rosseland approximation, radiation is expressed as:

$$q_r = -\frac{4\sigma^*}{3k^*} \frac{\partial \bar{T}^4}{\partial y}. \quad (7)$$

Utilizing the Taylor series expansions on T^4 while ignoring grater order terms:

$$\frac{\partial q_r}{\partial y} = -\frac{16}{3} \frac{\sigma^* \bar{T}_\infty^3}{k^*} \left(\frac{\partial^2 \bar{T}}{\partial y^2} \right). \quad (8)$$

Dimensional-less variables are considered in the corresponding manner [58]:

$$\begin{aligned} \bar{u} = bxf'(\eta), \bar{v} = -(bv)^{\frac{1}{2}} f(\eta), \psi = (bv)^{\frac{1}{2}} xf(\eta), \eta = \left(\frac{b}{v} \right)^{\frac{1}{2}} y, \\ \theta(\eta) = \frac{\bar{T} - \bar{T}_\infty}{\bar{T}_w - \bar{T}_\infty}, \phi(\eta) = \frac{\bar{C} - \bar{C}_\infty}{\bar{C}_w - \bar{C}_\infty}, \chi(\eta) = \frac{\bar{N} - \bar{N}_\infty}{\bar{N}_w - \bar{N}_\infty}. \end{aligned} \quad (9)$$

Utilizing the similarity variables (1-5) equations are transformed into the following ordinary differential equations:

$$f''' + \beta_1 (2ff'f'' - f'^2 f''') + \beta_2 (f''^2 - ff''''') - f'^2 + ff'' - (\lambda - M)f' + F_r f'^2 = 0, \quad (10)$$

$$\left(1 + \frac{4}{3Rd}\right)\theta'' + Pr(f\theta' + N_b\theta'\phi' + N_t\theta'^2 + Q\theta) = 0, \quad (11)$$

$$\phi'' + Lef(\eta)\phi' + \frac{N_t}{N_b}\theta'' = 0, \quad (12)$$

$$\chi'' + Lbf\chi' - Pe(\chi\phi'' + \omega\phi'' + \chi'\phi') = 0. \quad (13)$$

The boundary conditions are given listed below:

$$\begin{aligned} f(0) = 0, f'(0) = 1, \theta(0) = 1, \phi(0) = 1, \chi(0) = 1, \\ f'(\infty) \rightarrow 0, \theta(\infty) \rightarrow 0, \chi(\infty) \rightarrow 0, \phi(\infty) \rightarrow 0. \end{aligned} \quad (14)$$

The following equations have been determined.

$$C_f \cdot Re_x^{-\frac{1}{2}} = f''(0), Re_x^{-\frac{1}{2}} \cdot Nu_x = -\left(1 + \frac{4}{3Rd}\right)\theta'(0), Re_x^{-\frac{1}{2}} \cdot Sh_x = -\phi'(0), Re_x^{-\frac{1}{2}} \cdot Nn_x = -\chi'(0). \quad (15)$$

3. Methodology

3.1 Optimal Homotopy Analysis Method solution

The initial perturbation and auxiliary functions required for generating solutions using the context of the Optimal Homotopy analysis Method are specifically explained a described [54-56]:

$$f_0(\eta) = 1 - e^{-\eta}, \theta_0(\eta) = e^{-\eta}, \phi_0(\eta) = e^{-\eta}, \chi_0(\eta) = e^{-\eta}, \quad (16)$$

$$L_f(f) = \frac{d^3}{d\eta^3} - \frac{d}{d\eta}, L_\theta(\theta) = \frac{d^2\theta}{d\eta^2} - \theta, L_\phi(\phi) = \frac{d^2\phi}{d\eta^2} - \phi, L_\chi(\chi) = \frac{d^2\chi}{d\eta^2} - \chi. \quad (17)$$

The linear operators discussed before correspond to the required conditions:

$$\left. \begin{aligned} L_f \left[\tilde{B}_1^* + \tilde{B}_2^* e^\eta + \tilde{B}_3^* e^{-\eta} \right] = 0, L_\theta \left[\tilde{B}_4^* e^\eta + \tilde{B}_5^* e^{-\eta} \right] = 0, \\ L_\phi \left[\tilde{B}_6^* e^\eta + \tilde{B}_7^* e^{-\eta} \right] = 0, L_\chi \left[\tilde{B}_8^* e^\eta + \tilde{B}_9^* e^{-\eta} \right] = 0. \end{aligned} \right\} \quad (18)$$

In academia, the notation \tilde{B}_k^* where k ranges from 1 to 9, is employed to indicate unknown constants.

3.2 Convergence analysis for OHAM

The parameters $\mathfrak{h}, \mathfrak{h}_\theta, \mathfrak{h}_\phi$ and \mathfrak{h}_χ are vital for controlling convergence in homotopic solutions. They influence the size and velocity of convergence. To establish the best values for these parameters, a minimization strategy was used. This method involves improving the parameters via a technique first proposed by Liao [50], in which the squared averaged residual errors are modeled.

$$\epsilon_{\dot{m}}^f = \frac{1}{k+1} \sum_{j=0}^k \left[N_f \left(\sum_{i=0}^m \tilde{f}(\eta), \sum_{i=0}^m \tilde{\theta}(\eta), \right)_{\eta=j\delta\eta} \right]^2, \quad (19)$$

$$\epsilon_{\dot{m}}^\theta = \frac{1}{k+1} \sum_{j=0}^k \left[N_\theta \left(\sum_{i=0}^m \tilde{f}(\eta), \sum_{i=0}^m \tilde{\theta}(\eta), \right)_{\eta=j\delta\eta} \right]^2, \quad (20)$$

$$\epsilon_{\dot{m}}^\phi = \frac{1}{k+1} \sum_{j=0}^k \left[N_\phi \left(\sum_{i=0}^m \tilde{f}(\eta), \sum_{i=0}^m \tilde{\theta}(\eta), \sum_{i=0}^m \tilde{\phi}(\eta), \right)_{\eta=j\delta\eta} \right]^2, \quad (21)$$

$$\epsilon_{\dot{m}}^\chi = \frac{1}{k+1} \sum_{j=0}^k \left[N_\chi \left(\sum_{i=0}^m \tilde{f}(\eta), \sum_{i=0}^m \tilde{\theta}(\eta), \sum_{i=0}^m \tilde{\chi}(\eta), \right)_{\eta=j\delta\eta} \right]^2. \quad (22)$$

Following Liao [50]:

$$\epsilon_{\dot{m}}^t = \epsilon_{\dot{m}}^f + \epsilon_{\dot{m}}^\theta + \epsilon_{\dot{m}}^\phi + \epsilon_{\dot{m}}^\chi. \quad (23)$$

In the provided context, wherein $\epsilon_{\dot{m}}^t$ indicates the average square residual error. Setting $\delta\eta$ to 0.5 and \mathbf{K} to 30 results in optimal control variable values that converge at the 2nd order of distortions can be determined using the following parameters: $\mathbf{h}_f = -1.2338003$, $\mathbf{h}_\theta = -0.94407680$, $\mathbf{h}_\phi = -0.59920359$, $\mathbf{h}_\chi = 0.9723090613$, and $\epsilon_{\dot{m}}^t = 8.45285 \times 10^{-2}$.

4. Result and Discussion

In this section, the features of all the embedding physical parameters are highlighted. The graphs are plotted for velocity, temperature and concentration profiles for various values of parameters, fluid relaxation and retardation constant (β_1, β_2), Prandtl number (Pr), Magnetic parameter (M), Pectet factor (Pe), Brownian motion (N_b), Thermophoresis number (N_t), Lewis number (Lb), Heat radiation parameter (Q) etc.

Figs. 2-3 represents the influences of fluid relaxation and retardation (β_1, β_2), on velocity profile as other parameters remain constant ($M = 0.2, \lambda = 0.3, F_r = 0.5, Lb = 0.4, Rd = 0.2, N_b = 0.1, Q = 0.2, N_t = 0.2, Le = 0.2, \omega = 0.2 \& Pe = 0.3$). It

has seemed that there is a decline in velocity profile by the increase in fluid relaxation time. Since the fluid mobility is increased by the retardation of fluid. So, the velocity profile increases with the increase (β_2). Figs. 4-5 shows that as rotational parameter λ and magnetic field M increase there is drops in velocity distribution as other parameters remain same ($\beta_1 = 0.2, Q = 0.2, \beta_2 = 0.1, F_r = 0.5, N_b = 0.1, Le = 0.2, Rd = 0.2, N_t = 0.2, Lb = 0.4, Pe = 0.3$ and $\omega = 0.2$). The thickness of the momentum barrier layer decreases as a result of the increase in the rotational parameter and the magnetic parameter. Practically, decrease in the boundary layer's velocity distribution by a rise in the values of λ and M result from the warmth fluid being transferred in the direction of the stretched surface. Moreover, when taking into account the magnetic parameter, the fluid's motion brought on by the sheet's stretching is what causes a drop in the velocity distribution at the sheet's surface, this is managed by applying a magnetic field because it produces a drag-like force more precisely, the Lorentz force that has the ability to reduce the fluid motion in the boundary layer. In Fig. 6 it seems that when the Forchheimer number increases, the velocity distribution does also. Fig. 7 demonstrates how thermal radiation affects temperature fields. In this situation, thermal energy is increased by the utilization of thermal radiation. When thermal radiation is used, they are converted into heat energy. Thermal radiation is used to generate the largest amount of heat energy into fluidic particles. Increased radiation leads to thinner thermal layers. Furthermore, the temperature profile grows with the influence of thermal radiation parameters. The Prandtl number, defined as the ratio of momentum diffusivity to thermal diffusivity, is a dimensionless number used in fluid dynamics and transferring heat. As indicated by Figure 8, the distribution of Prandtl number results in a decline in fluid temperature. As a result, grow in Pr leads to a shift in thermal layers. As a consequence, the function of thermal layers declines as the Prandtl number Pr increases. Pr is the ratio of heat layers to momentum layers. The quantity of heat energy generated decreases as the Prandtl number increases. As a result, fluidic temperature decreases as the Prandtl number increases. Fig. 9-10 illustrates the variation thermophoretic parameters N_t , as well as the effects of heat generation and absorption Q as other parameter remain constant ($\beta_1 = 0.2, \beta_2 = 0.1, M = 0.2, \lambda = 0.3, F_r = 0.5, N_b = 0.1, Le = 0.2, Lb = 0.4, \omega = 0.2$ & $Pe = 0.3$), all have an impact on the temperature of the thermal boundary layers. It has been found that by increasing these parameters there is an increment in temperature profile. Fig. 11-13 represents that as Lewis number Le and Brownian motion number N_b increase, nanoparticle concentration decreases and in Fig. 12 it has

been seen that as thermophoresis number N_t increases, there is an enhancement in concentration profile. The result concludes that the only area in which the nanoparticle concentration is significantly influenced by the Lewis number and Brownian motion parameter is near the stretching sheet. This is due to the profile's propensity to meet farther apart until their values are zero. Fig. 14-15 demonstrates that when the bioconvection Lewis number Lb increases, the quantity of motile microorganisms increases. Fig. 16 indicates how the motility distribution ω falls as the Peclet factor Pe rise.

Table 1 illustrates the squared averaged individual residual error for different approximation orders using the ideal numbers from the auxiliary parameters. Table 2 depicts the influence of β_1, β_2 and M on skin friction when $Rd = 0.2, Pe = 0.3, N_t = 0.2, Le = 0.2, Pr = 1.0, Q = 0.2, Lb = 0.4, \text{ and } \omega = 0.2$. There is an increment in skin friction when β_1 increases and skin friction decreases by increases of β_2 . Table 3 shows the impact of N_t and Q on Nusselt number, when $M = 0.2, Lb = 0.4, \gamma = 0.3, Rd = 0.2, \omega = 0.2, F_r = 0.5, Pr = 1.0, Le = 0.2 \text{ and } Pe = 0.3$. By increasing N_t and Q , Nusselt number decreases. Table 4 represent the influence of Sherwood number. Table 5 shows the effects of ω and Lb on $-\chi'(0)$, when $M = 0.2, N_t = 0.2, Rd = 0.2, F_r = 0.5, Pr = 1.0, \gamma = 0.3, Le = 0.2, Pe = 0.3$ and $Q = 0.2$. By increasing ω Nusselt number also increases and by increasing Bioconvection Lewis number the Nusselt number decreases. Table 6 displays the influence of comparison findings on Nusselt number.

5. Conclusion

The OHAM evaluation of the Oldroyd-B nanofluid flow across a stretching sheet shows that thermal radiation improves heat transfer and internal heat generation increases thermal efficiency. The Darcy-Forchheimer model demonstrates how porous medium resistance slows fluid velocity and influences temperature and concentration profiles. MHD effects change flow dynamics, with greater magnetic fields reducing velocity and increasing heat conductivity. Bio-convective factors influence nanoparticle distribution. The study supports OHAM's accuracy and emphasizes its utility in improving industrial procedures involving nanofluids and stretched surfaces, underlining the need of taking thermal radiation, heat generation, and MHD into account in real-world applications. The

following findings are based on the current investigation.

- Raising the fluid relaxation time number and magnetic number near the stretching sheet leads to a decline in the velocity distribution and Forchheimer number have the opposite effect;
- Near the stretching sheet, the velocity profile drops as the slip parameter λ grows.
- The temperature profile in the thermal boundary layer improves with a rise in the amount of thermal radiation and Q , but the reverse trend is found in the value of the Pr .
- The Brownian motion parameter N_t and Lewis number Le and demonstrate a decrease in concentration on the stretching surface. The N_t displays a reverse trend;
- Raising the Peclet factor. The motility distribution reduces with Pe and ω , whereas increasing the bioconvection Lewis number Lb has the opposite result.

Nomenclature

Abbreviation	Full name	Abbreviation	Full name
(\vec{u}, \vec{v})	Velocity components $m s^{-1}$	Lb	Lewis number
Pe	Peclet factor	β_1	Fluid relaxation time number
D_T	Thermophoresis diffusion coefficient $m^2 s^{-1}$	F_r	Forchheimer number
μ	Dynamic viscosity $kg / m.s$	\vec{C}	Concentration K
Rd	Thermal radiation parameter	Le	Lewis number
β_1	Fluid relaxation time number	Q	Heat generation/absorption
x, y	Coordinates axis $m s^{-1}$	Pr	Prandtl number
ρ_p	Density of the particle $kg m^{-3}$	β_2	Fluid retardation time number

ρ	Fluid density kg / m^3	N_b	Brownian motion factor
\bar{T}	Temperature K	k	Thermal conductivity $W m^{-1} K^{-1}$
D_B	Brownian diffusion coefficient $m^2 s^{-1}$	α	Thermal diffusivity $m^2 s^{-1}$
M	Magnetic factor	N_t	Thermophoretic parameter
ν	Kinematic viscosity $m^2 s^{-1}$	λ	slip parameter

Availability of data and material: The datasets utilized and/or evaluated during the current investigation are available upon reasonable request from the corresponding author.

Conflict of Interest: The authors disclose no competing interest.

References

1. M. Usman, et al., “Heat transfer distribution in Oldroyd-B nanofluid with variable thermal conductivity: a fractional approach,” *Case Stud. Therm. Eng.*, vol. 52, pp. 103762, DOI: <https://doi.org/10.1016/j.csite.2023.103762>, (2023).
2. Tang, T. Q., Rooman, M., Shah, Z., et al. “Computational study and characteristics of magnetized gold-blood Oldroyd-B nanofluid flow and heat transfer in stenosis narrow arteries”, *Journal of Magnetism and Magnetic Materials*, 569, 170448. DOI: <https://doi.org/10.1016/j.jmmm.2023.170448>, (2023).
3. Cao, W., Kaleem, M. M., Usman, M., et al. “A study of fractional Oldroyd-B fluid between two coaxial cylinders containing gold nanoparticles”, *Case Studies in Thermal Engineering*, 45, 102949. DOI: <https://doi.org/10.1016/j.csite.2023.102949>.
4. Ameer Ahammad, N., Veera Krishna, M., & Algehyne, E. A. “Heat and mass transfer on unsteady MHD flow of Casson fluid over an infinite perpendicular absorbent plate with slip effects”. *Heat Transfer*, 51(7), 6685-6704. DOI: <https://doi.org/10.1002/htj.22618>, (2022).
5. Rosmila, A. B., Kandasamy, R., & Muhaimin, I. “Lie symmetry group transformation for MHD natural convection flow of nanofluid over linearly porous stretching sheet in presence of thermal stratification”. *Applied Mathematics and Mechanics*, 33, 593-604. DOI: <https://doi.org/10.1007/s10483-012-1573-9>, (2012).
6. Jawad, M., Saeed, A., Khan, A., et al. “Unsteady bioconvection Darcy-Forchheimer nanofluid flow through a horizontal channel with impact of magnetic field and thermal radiation”. *Heat Transfer*, 50(4), 3240-3264. DOI: <https://doi.org/10.1002/htj.22026>, (2021).
7. Ellahi, R. “The effects of MHD and temperature dependent viscosity on the flow of non-Newtonian nanofluid in a pipe: analytical solutions”. *Applied Mathematical Modelling*, 37(3), 1451-1467. DOI: <https://doi.org/10.1016/j.apm.2012.04.004>, (2013).

8. Khan, S. U., & Ali, H. M. "Swimming of gyrotactic microorganisms in unsteady flow of Eyring Powell nanofluid with variable thermal features: Some bio-technology applications". *International Journal of Thermophysics*, 41, 1-19. DOI: <https://doi.org/10.1007/s10765-020-02736-2>, (2020).
9. Chu, Y. M., Aziz, S., Khan, M. I., et al. "Nonlinear radiative bioconvection flow of Maxwell nanofluid configured by bidirectional oscillatory moving surface with heat generation phenomenon". *Physica scripta*, 95(10), 105007. DOI: [10.1088/1402-4896/abb7a9](https://doi.org/10.1088/1402-4896/abb7a9), (2020).
10. Khan, S. U., Al-Khaled, K., & Bhatti, M. M. "Bioconvection analysis for flow of Oldroyd-B nanofluid configured by a convectively heated surface with partial slip effects". *Surfaces and Interfaces*, 23, 100982. DOI: <https://doi.org/10.1016/j.surfin.2021.100982>, (2021).
11. Ramzan, M., Chung, J. D., & Ullah, N. "Radiative magnetohydrodynamic nanofluid flow due to gyrotactic microorganisms with chemical reaction and non-linear thermal radiation". *International Journal of Mechanical Sciences*, 130, 31-40. DOI: <https://doi.org/10.1016/j.ijmecsci.2017.06.009>, (2017).
12. Alshomrani, A. S., Ullah, M. Z., & Baleanu, D. "Importance of multiple slips on bioconvection flow of cross nanofluid past a wedge with gyrotactic motile microorganisms". *Case Studies in Thermal Engineering*, 22, 100798. DOI: <https://doi.org/10.1016/j.csite.2020.100798>, (2020).
13. Nadeem, S., Ijaz, M., El-Kott, A., et al. "Rosseland analysis for ferromagnetic fluid in presence of gyrotactic microorganisms and magnetic dipole". *Ain Shams Engineering Journal*, 11(4), 1295-1308. DOI: <https://doi.org/10.1016/j.asej.2020.03.007>, (2020).
14. Elayarani, M., Shanmugapriya, M., & Kumar, P. S. "Intensification of heat and mass transfer process in MHD carreau nanofluid flow containing gyrotactic microorganisms". *Chemical Engineering and Processing-Process Intensification*, 160, 108299. DOI: <https://doi.org/10.1016/j.cep.2021.108299>, (2021).
15. Shehzad, S. A., Mushtaq, T., Abbas, Z., et al. "Dynamics of bioconvection flow of micropolar nanoparticles with Cattaneo-Christov expressions". *Applied Mathematics and Mechanics*, 41, 1333-1344. DOI: <https://doi.org/10.1007/s10483-020-2645-9>, (2020).

16. Khan, M. I., Waqas, H., Khan, S. U., et al. "Slip flow of micropolar nanofluid over a porous rotating disk with motile microorganisms, nonlinear thermal radiation and activation energy". *International Communications in Heat and Mass Transfer*, 122, 105161. DOI: <https://doi.org/10.1016/j.icheatmasstransfer.2021.105161>, (2021).
17. Kuznetsov, A. V. "The onset of nanofluid bioconvection in a suspension containing both nanoparticles and gyrotactic microorganisms". *International Communications in Heat and Mass Transfer*, 37(10), 1421-1425. DOI: <https://doi.org/10.1016/j.icheatmasstransfer.2010.08.015>, (2010).
18. Waqas, H., Khan, S. U., Hassan, M., et al. "Analysis on the bioconvection flow of modified second-grade nanofluid containing gyrotactic microorganisms and nanoparticles". *Journal of Molecular Liquids*, 291, 111231. DOI: <https://doi.org/10.1016/j.molliq.2019.111231>, (2019).
19. Khan, S. U., Al-Khaled, K., & Khan, M. I. "Convective nonlinear thermally developed flow of thixotropic nanoliquid configured by Riga surface with gyrotactic microorganism and activation energy: A bio-technology and thermal extrusion model". *International Communications in Heat and Mass Transfer*, 119, 104966. DOI: <https://doi.org/10.1016/j.icheatmasstransfer.2020.104966>, (2020).
20. Irfan, M., Khan, M., Khan, W. A., et al. "Influence of thermal-solutal stratifications and thermal aspects of non-linear radiation in stagnation point Oldroyd-B nanofluid flow". *International Communications in Heat and Mass Transfer*, 116, 104636. DOI: <https://doi.org/10.1016/j.icheatmasstransfer.2020.104636>, (2020).
21. Alzahrani, F., Gowda, R. P., Kumar, R. N., et al. "Dynamics of thermosolutal Marangoni convection and nanoparticle aggregation effects on Oldroyd-B nanofluid past a porous boundary with homogeneous-heterogeneous catalytic reactions". *Journal of the Indian Chemical Society*, 99(6), 100458. DOI: <https://doi.org/10.1016/j.jics.2022.100458>, (2022).
22. Almakki, M., Nandy, S. K., Mondal, S., et al. "A model for entropy generation in stagnation-point flow of non-Newtonian Jeffrey, Maxwell, and Oldroyd-B nanofluids". *Heat Transfer—Asian Research*, 48(1), 24-41. DOI: <https://doi.org/10.1002/htj.21366>, (2019).

23. Ramzan, M., Howari, F., Chung, J. D., et al. “Irreversibility minimization analysis of ferromagnetic Oldroyd-B nanofluid flow under the influence of a magnetic dipole”. *Scientific Reports*, 11(1), 4810. DOI: <https://doi.org/10.1038/s41598-021-84254-1>, (2021).
24. Sarada, K., Gowda, R. J. P., Sarris, I. E., et al. “Effect of magnetohydrodynamics on heat transfer behaviour of a non-Newtonian fluid flow over a stretching sheet under local thermal non-equilibrium condition”. *Fluids*, 6(8), 264. DOI: <https://doi.org/10.3390/fluids6080264>, (2021).
25. Khan, M. N., Nadeem, S., Ullah, N., et al. “Theoretical treatment of radiative Oldroyd-B nanofluid with microorganism pass an exponentially stretching sheet”. *Surfaces and Interfaces*, 21, 100686. DOI: <https://doi.org/10.1016/j.surfin.2020.100686>, (2020).
26. Ramzan, M., Farooq, M., Alhothuali, M. S., et al. “Three-dimensional flow of an Oldroyd-B fluid with Newtonian heating”. *International Journal of Numerical Methods for Heat & Fluid Flow*, 25(1), 68-85. DOI: <https://doi.org/10.1108/HFF-03-2014-0070>, (2015).
27. Bilal Ashraf, M., Hayat, T., & Alsulami, H. “Mixed convection Falkner-Skan wedge flow of an Oldroyd-B fluid in presence of thermal radiation”. *Journal of Applied Fluid Mechanics*, 9(4), 1753-1762. DOI: [10.18869/acadpub.jafm.68.235.24323](https://doi.org/10.18869/acadpub.jafm.68.235.24323), (2016).
28. Sohail, M., Naz, R., & Bilal, S. “Thermal performance of an MHD radiative Oldroyd-B nanofluid by utilizing generalized models for heat and mass fluxes in the presence of bioconvective gyrotactic microorganisms and variable thermal conductivity”. *Heat Transfer—Asian Research*, 48(7), 2659-2675. DOI: <https://doi.org/10.1002/htj.21475>, (2019).
29. Sandeep, N., Kumar, B. R., & Kumar, M. J. “A comparative study of convective heat and mass transfer in non-Newtonian nanofluid flow past a permeable stretching sheet”. *Journal of Molecular Liquids*, 212, 585-591. DOI: <https://doi.org/10.1016/j.molliq.2015.10.010>, (2015).
30. Hayat, T., Waqas, M., Shehzad, S. A., et al. “On 2D stratified flow of an Oldroyd-B fluid with chemical reaction: an application of non-Fourier heat flux theory”. *Journal of Molecular Liquids*, 223, 566-571. DOI: <https://doi.org/10.1016/j.molliq.2016.08.083>, (2016).

31. Waqas, M., et al. "Stratified flow of an Oldroyd-B nanoliquid with heat generation." *Results in physics*, 7, 2489-2496. DOI: <https://doi.org/10.1016/j.rinp.2017.06.030>, (2017).
32. Magesh, A., Tamizharasi, P. and Vijayaragavan, R., "Non-Newtonian fluid flow with the influence of induced magnetic field through a curved channel under peristalsis". *Heat Transfer*, 52(7), pp.4946-4961. DOI: <https://doi.org/10.1002/htj.22912>, (2023).
33. Magesh, A., Pushparaj, V., Srinivas, S. et al. "Numerical investigations of activation energy on the peristaltic transport of Carreau nanofluid through a curved asymmetric channel". *Physics of Fluids*, 35(10). DOI: <https://doi.org/10.1063/5.0167829>, (2023).
34. Magesh, A., Tamizharasi, P. and Kamalakkannan, J., "Analysis of Bejan number and Entropy generation of Non-Newtonian nanofluid through an asymmetric microchannel". *Numerical Heat Transfer, Part A: Applications*, pp.1-17. DOI: <https://doi.org/10.1080/10407782.2023.2240507>, (2023).
35. Magesh, A., Tamizharasi, P., Makinde, O.D. et al. "Analysis of activation energy on the Johnson–Segalman nanofluid through an asymmetric microchannel: Numerical study". *International Journal of Modern Physics B*, p.2550019. DOI: <https://doi.org/10.1142/S0217979225500195>, (2024).
36. Praveen Kumar, P., Balakrishnan, S., Magesh, A., et al. "Numerical treatment of entropy generation and Bejan number into an electroosmotically-driven flow of Sutterby nanofluid in an asymmetric microchannel". *Numerical Heat Transfer, Part B: Fundamentals*, pp.1-20. DOI: <https://doi.org/10.1080/10407790.2024.2329773>, (2024).
37. Akbar, Y., Huang, S., Magesh, A., et al. "Thermal analysis of mixed convective peristaltic pumping of nanofluids in the occurrence of an induced magnetic field and variable viscosity". *Journal of Taibah University for Science*, 18(1), p.2319890. DOI: <https://doi.org/10.1080/16583655.2024.2319890>, (2024).
38. Kezzar, M., Dib, A., Ayub, A., et al. "Duan Rach approach solution of MHD flow of ternary hybrid Casson magnetized nanofluid in converging/diverging geometry with velocity slip effects". *Numerical Heat Transfer, Part A: Applications*, pp.1-18. DOI: <https://doi.org/10.1080/10407782.2024.2360654>, (2024).

39. Ayub, A., Iqbal, Z., Shah, S.Z.H., et al. “Neural intelligent approach for heat transfer applications of trihybrid cross bio-nanofluid over wedge geometry”. *Modern Physics Letters B*, p.2450439. DOI: <https://doi.org/10.1142/S0217984924504396>, (2024).
40. Ayub, A., Shah, S.Z.H., Sabir, Z., et al. “A novel study of the Cross nanofluid with the effects of inclined magnetic field in fuzzy environment”. *International Journal of Thermofluids*, 22, p.100636. DOI: <https://doi.org/10.1016/j.ijft.2024.100636>, (2024).
41. Hussain Shah, S.Z., Ayub, A., Khan, U., et al. “Thermal transport exploration of ternary hybrid nanofluid flow in a non-Newtonian model with homogeneous-heterogeneous chemical reactions induced by vertical cylinder”. *Advances in Mechanical Engineering*, 16(5), p.16878132241252229. DOI: <https://doi.org/10.1177/16878132241252229>, (2024).
42. Alqudah, M., Shah, S.Z.H., Riaz, M.B., et al. “Neural network architecture to optimize the nanoscale thermal transport of ternary magnetized Carreau nanofluid over 3D wedge”. *Results in Physics*, 59, p.107616. DOI: <https://doi.org/10.1016/j.rinp.2024.107616>, (2024).
43. Shamshuddin, M.D., Saeed, A., Mishra, S.R., et al. “Homotopic simulation of MHD bioconvective flow of water-based hybrid nanofluid over a thermal convective exponential stretching surface”. *International Journal of Numerical Methods for Heat & Fluid Flow*, 34(1), pp.31-53. DOI: <https://doi.org/10.1108/HFF-03-2023-0128>, (2024).
44. Shamshuddin, M.D., Salawu, S.O., Ramesh, K., et al. “Bioconvective treatment for the reactive Casson hybrid nanofluid flow past an exponentially stretching sheet with Ohmic heating and mixed convection”. *Journal of Thermal Analysis and Calorimetry*, 148(21), pp.12083-12095. DOI: <https://doi.org/10.1007/s10973-023-12465-x>, (2023).
45. Lone, S.A., Shamshuddin, M.D., Shahab, S., et al. “Computational analysis of MHD driven bioconvective flow of hybrid Casson nanofluid past a permeable exponential stretching sheet with thermophoresis and Brownian motion effects”. *Journal of Magnetism and Magnetic Materials*, 580, p.170959. DOI: <https://doi.org/10.1016/j.jmmm.2023.170959>, (2023).
46. Gamar, F., Shamshuddin, M.D., Ram, M.S., et al. “Arrhenius evaluation of thermal radiative flux and energy for flowing micropolar nanofluid at stagnation point: a case of

- thermal study”. *Journal of Thermal Analysis and Calorimetry*, pp.1-11. DOI: <https://doi.org/10.1007/s10973-024-13132-5>, (2024).
47. Kandasamy, R., Loganathan, P., & Arasu, P. P. “Scaling group transformation for MHD boundary-layer flow of a nanofluid past a vertical stretching surface in the presence of suction/injection”. *Nuclear Engineering and Design*, 241(6), 2053-2059. DOI: <https://doi.org/10.1016/j.nucengdes.2011.04.011>, (2011).
48. Sohail, M., Rafique, E., Singh, A., et al. “Engagement of modified heat and mass fluxes on thermally radiated boundary layer flow past over a stretched sheet via OHAM analysis”. *Discover Applied Sciences*, 6(5), 240. DOI: <https://doi.org/10.1007/s42452-024-05833-1>, (2024).
49. Wang, C. Y. “Free convection on a vertical stretching surface”, *ZAMM-Journal of Applied Mathematics and Mechanics/Zeitschrift für Angewandte Mathematik und Mechanik*, 69(11), 418-420. DOI: <https://doi.org/10.1002/zamm.19890691115>, (1989).
50. Liao, S. “An optimal homotopy-analysis approach for strongly nonlinear differential equations”, *Communications in Nonlinear Science and Numerical Simulation*, 15(8), pp. 2003-2016. DOI: <https://doi.org/10.1016/j.cnsns.2009.09.002>, (2010).
51. Sohail, M., Ilyas, K., Rafique, E., et al. “OHAM Analysis on Bio-convective Flow of Partial Differential Equations of Casson Nanofluid Under Thermal Radiation Impact Past over a Stretching Sheet”, *BioNanoScience*, 1-11. DOI: <https://doi.org/10.1007/s12668-024-01329-9>, (2024).
52. Saeed Khan, N., Shah, Q., & Sohail, A. “Dynamics with Cattaneo–Christov heat and mass flux theory of bioconvection Oldroyd-B nanofluid”, *Advances in Mechanical Engineering*, 12(8), DOI: <https://doi.org/10.1177/1687814020930464>, (2020).
53. Roy, N., & Pal, D. “Influence of activation energy and nonlinear thermal radiation with ohmic dissipation on heat and mass transfer of a Casson nanofluid over stretching sheet”, *Journal of Nanofluids*, 11(6), 819-832. DOI: <https://doi.org/10.1166/jon.2022.1882>, (2022).
54. Rafique, E., Ilyas, N., & Sohail, M. “Utilization of generalized heat flux model on thermal transport of powell-eyring model via oham with heat geneartion aspects: thermal transport of powell-eyring model”, *Babylonian Journal of Mathematics*, 2024, 19-33. DOI: <https://doi.org/10.58496/BJM/2024/003>, (2024).

55. Abbas, S. T., Rafique, E., Haider, I., & Sohail, M. “Utilization of OHAM on mixed convective flow of Williamson fluid model with viscous dissipation over a stretched cylinder”, *UNEC Journal of Engineering and Applied Sciences*, 4(1), 20-36. DOI: <https://doi.org/10.61640/ujeas.2024.0502>, (2024).
56. Sohail, M., & Abbas, S. T. “Utilization of variable thermal conductivity and diffusion coefficient on non-Newtonian Prandtl model with modified heat and mass fluxes”, *Multidiscipline Modeling in Materials and Structures*, 20(2), 317-340. DOI: <https://doi.org/10.1108/MMMS-10-2023-0328>, (2024).
57. Pal, D., & Roy, N. “Influence of Brownian motion and thermal radiation on heat transfer of a nanofluid over stretching sheet with slip velocity”, *International Journal of Applied and Computational Mathematics*, 3, 3355-3377. DOI: <https://doi.org/10.1007/s40819-016-0303-3>, (2017).
58. Ali, M. H., Abbas, S. T., Sohail, M., et al. “Study of Bioconvection Phenomenon in Jefferey Model in a Darcy-Forchheimer Porous Medium”, *BioNanoScience*, 1-13. DOI: <https://doi.org/10.1007/s12668-024-01412-1>, (2024).

Dr. MUHAMMAD SOHAIL belongs to a very small village of district Haripur, Khyber Pakhtunkhwa, Pakistan. He got his PhD Mathematics degree from the Institute of Space Technology Islamabad, Pakistan in 2020. Currently, he is working as an Assistant Professor Mathematics at Khwaja Fareed University of Engineering and Information Technology Rahim Yar Khan, Pakistan. His research interests are on CFD simulation, mass transport, heat transfer, mathematical modelling, nonlinear dynamics, stability analysis, numerical and analytical methods, fractional differential equations, mixed convection and heat exchangers. He has published more than about 170 research articles in different peer reviewed international journals. He has participated in many international and national events as a participant and as a speaker.

Komal Ilyas has completed MS Mathematics from Khwaja Fareed University of Engineering and Information Technology Rahim Yar Khan, Pakistan and her interest is in fluid mechanics. She is actively participating in different seminars and conferences on fluid mechanics topics. She is the author of one research publication. She is looking for the PhD position in applied mathematics.

Esha Rafique has completed MS Mathematics under the supervision of Dr. Muhammad Sohail from Khwaja Fareed University of Engineering and Information Technology Rahim Yar Khan, Pakistan and her interest is in applied mathematics and in fluid mechanics. She has published about 10 research papers in different well reputed international journals.

Shah Jahan is working as an Assistant Professor Mathematics at Khwaja Fareed University of Engineering and Information Technology Rahim Yar Khan, Pakistan. He is the author of about 50 research articles. He has a vast teaching and research experience. He has delivered lectures in different national and international conferences.

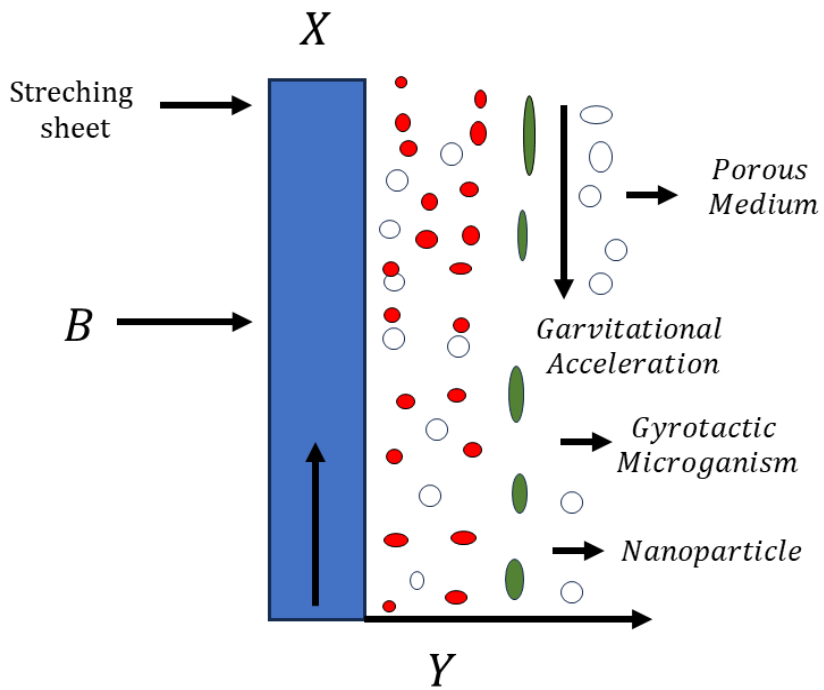


Fig. 1. Flow Geometry.

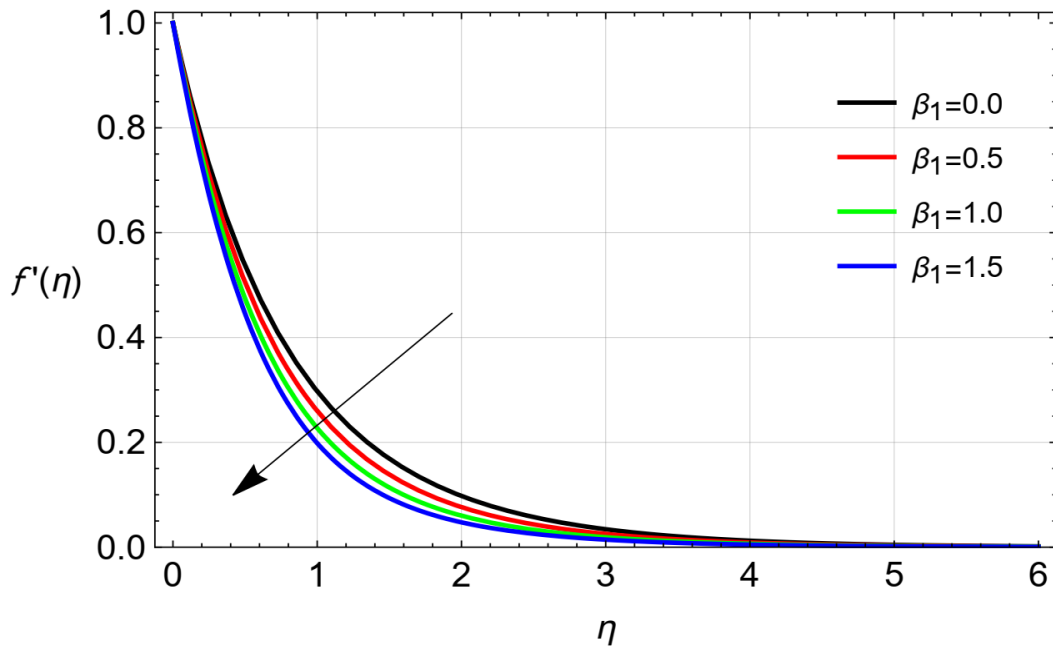


Fig. 2. Draw $f'(\eta)$ with a varying value of β_1 .

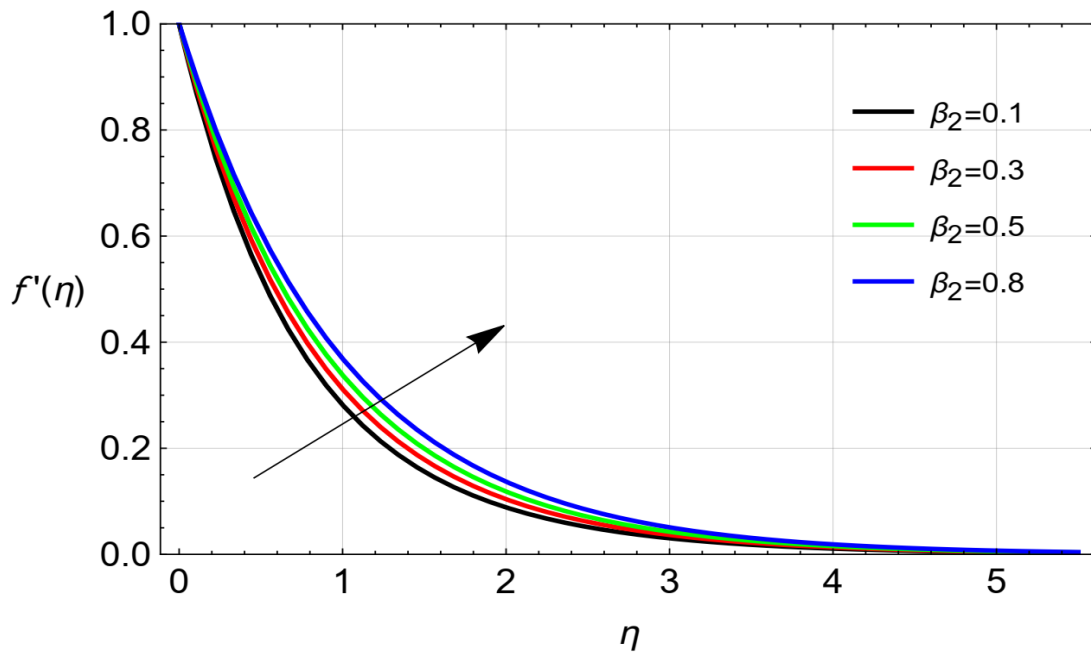


Fig. 3. Draw $f'(\eta)$ with a rising value of β_2 .

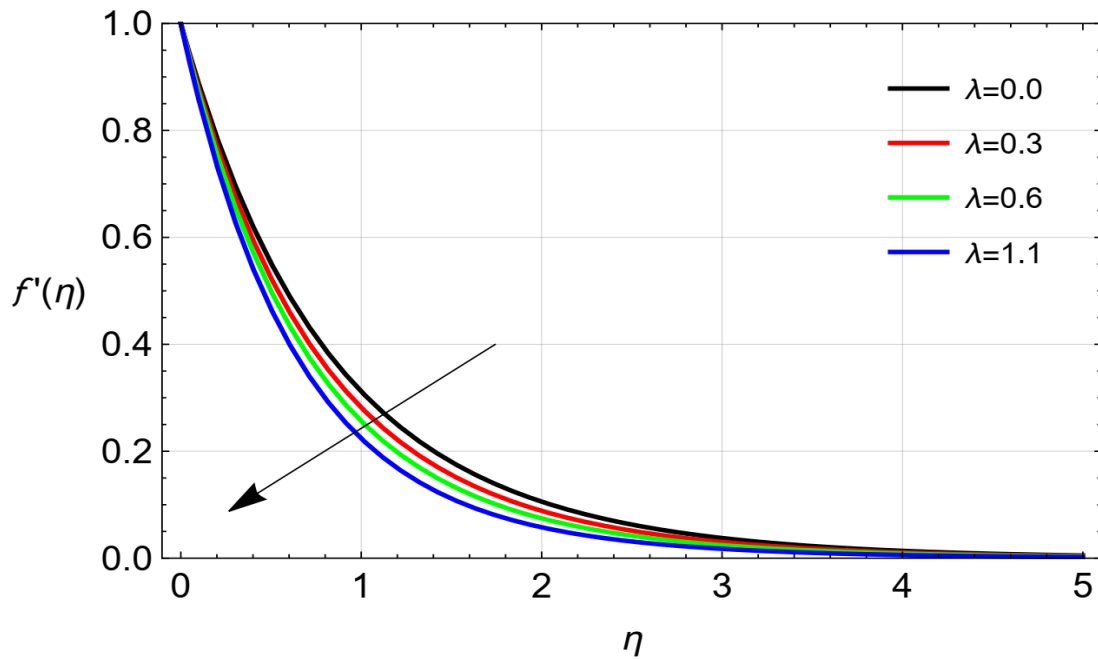


Fig. 4. Draw $f'(\eta)$ with a varying value of λ .

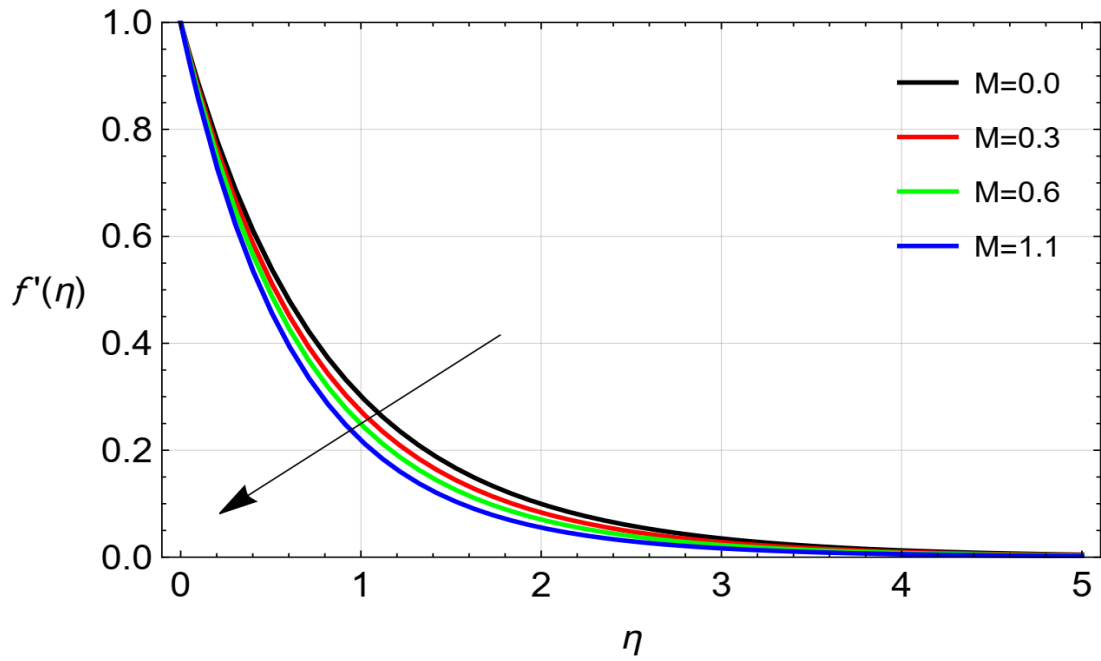


Fig. 5. Draw $f'(\eta)$ with a varying value of M .

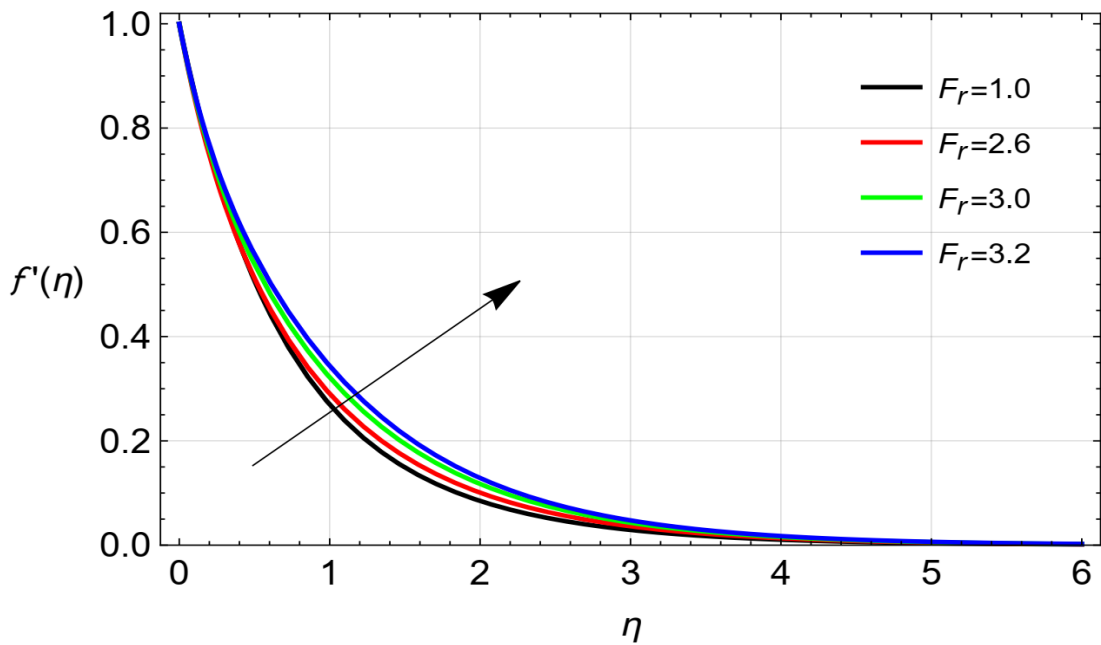


Fig. 6. Draw $f'(\eta)$ with a rising value of F_r .

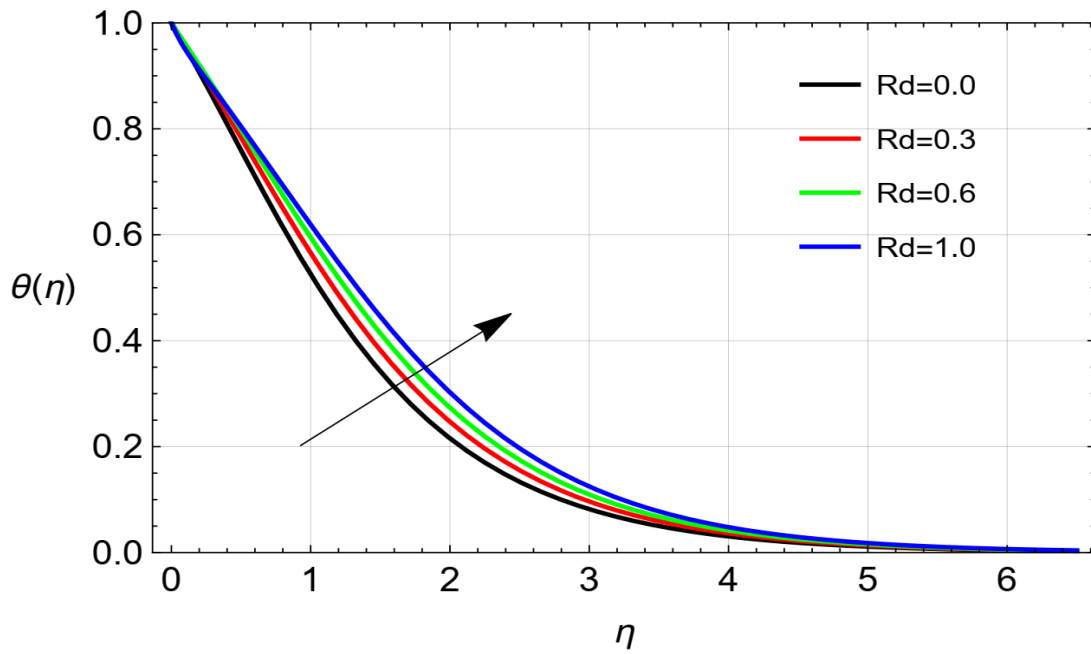


Fig. 7. Draw $\theta(\eta)$ with a rising value of Rd .

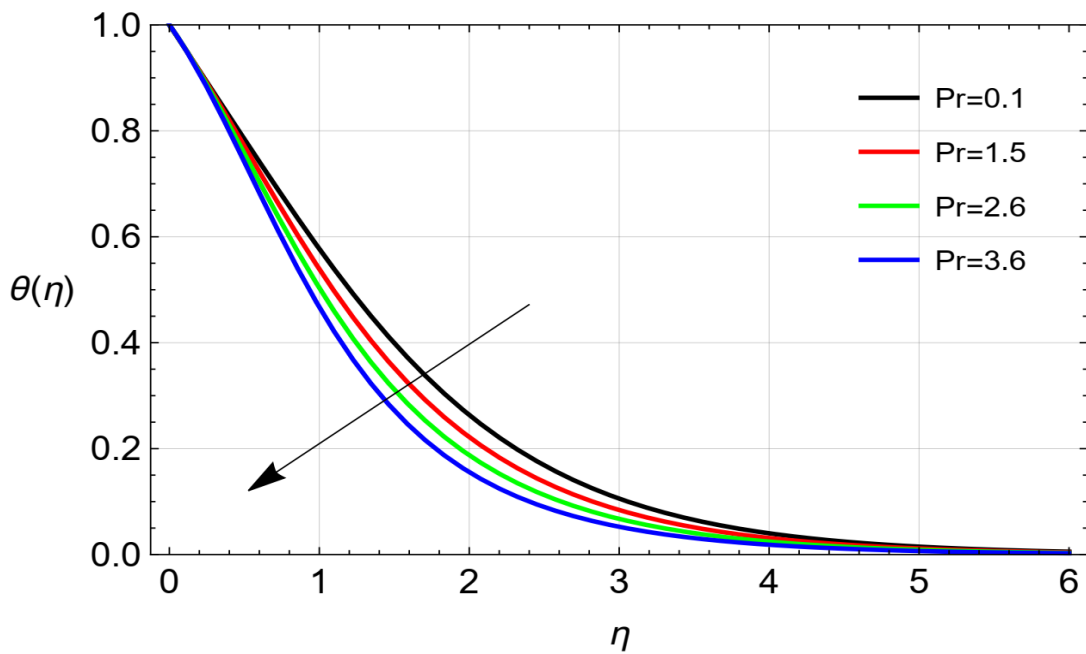


Fig. 8. Draw $\theta(\eta)$ with a varying value of Pr .

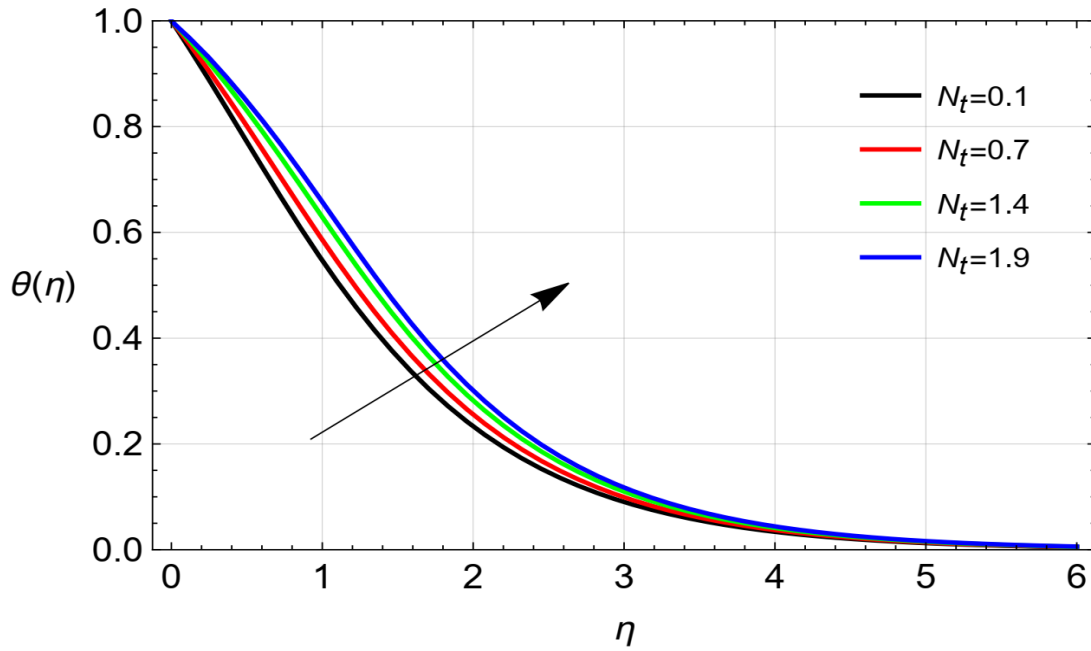


Fig. 9. Draw $\theta(\eta)$ with a rising value of N_t .

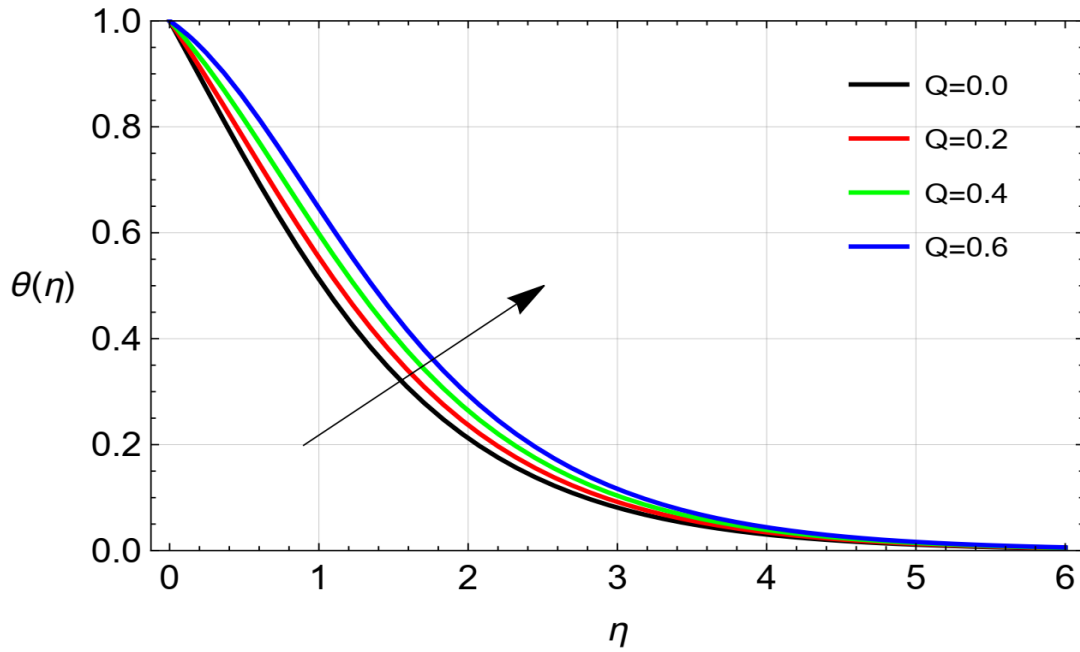


Fig. 10. Draw $\theta(\eta)$ with a rising value of Q .

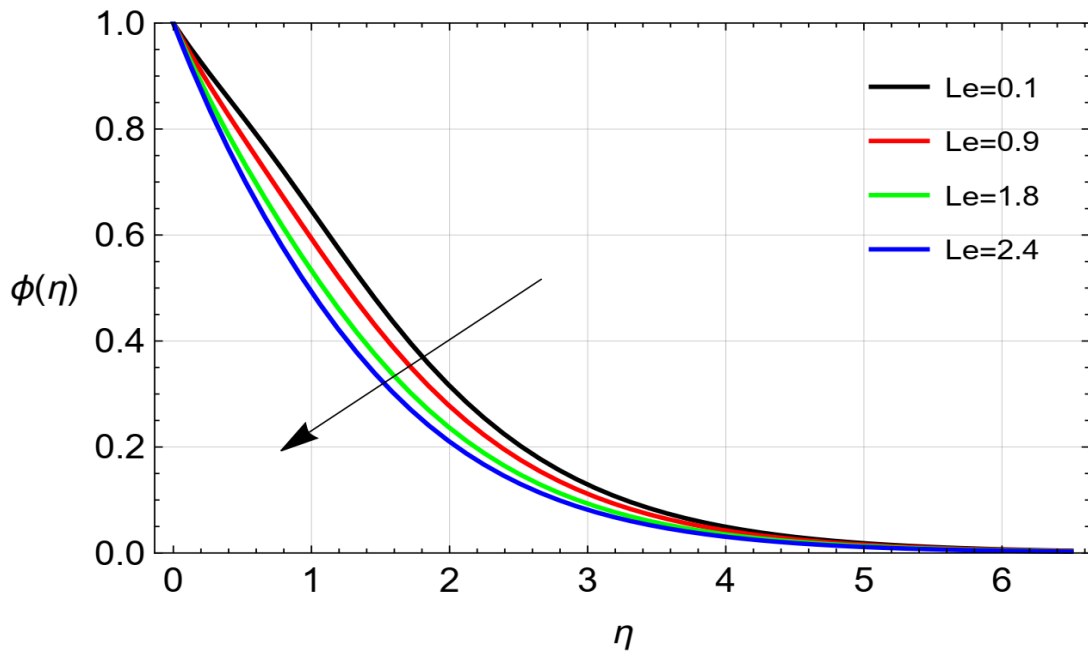


Fig. 11. Draw $\phi(\eta)$ with a varying value of Le

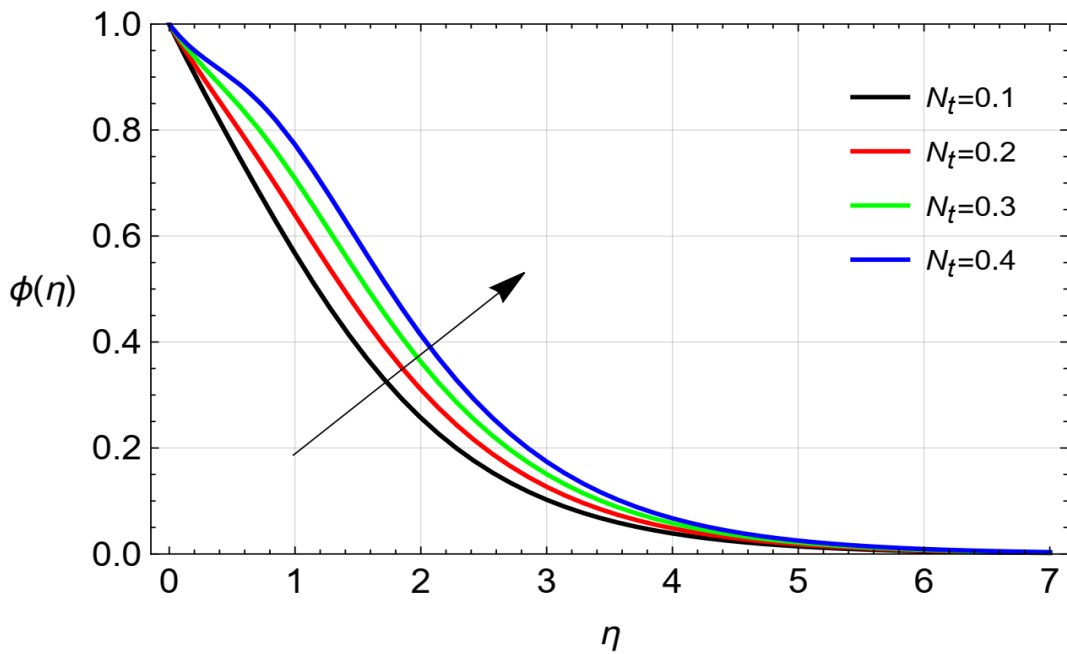


Fig. 12. Draw $\phi(\eta)$ with a rising value of N_t .

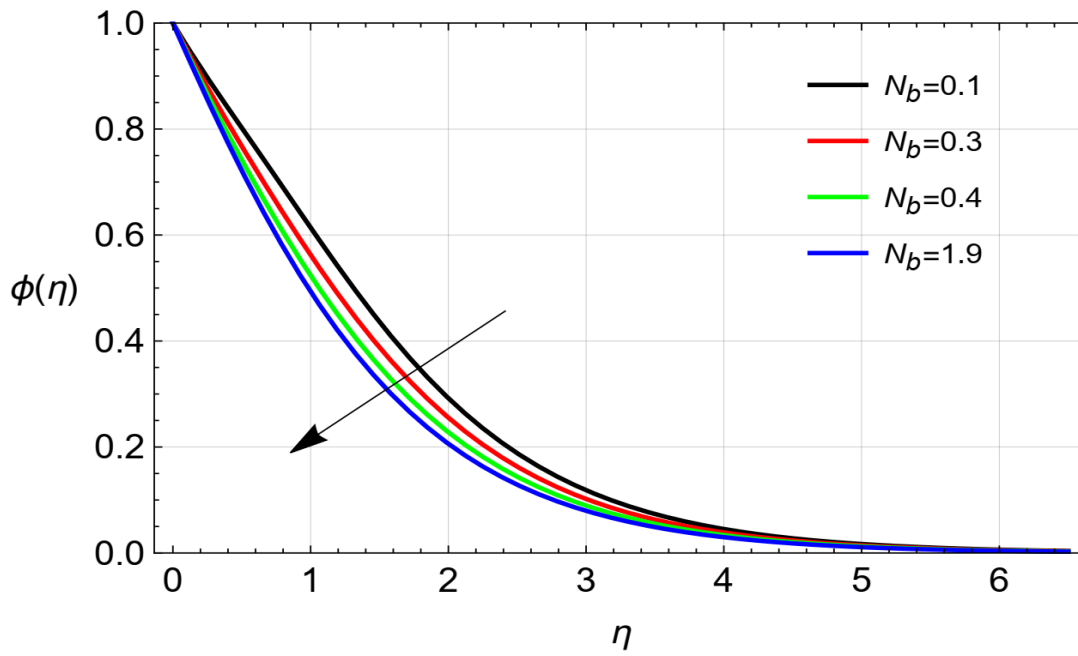


Fig. 13. Draw $\phi(\eta)$ with a varying value of N_b .

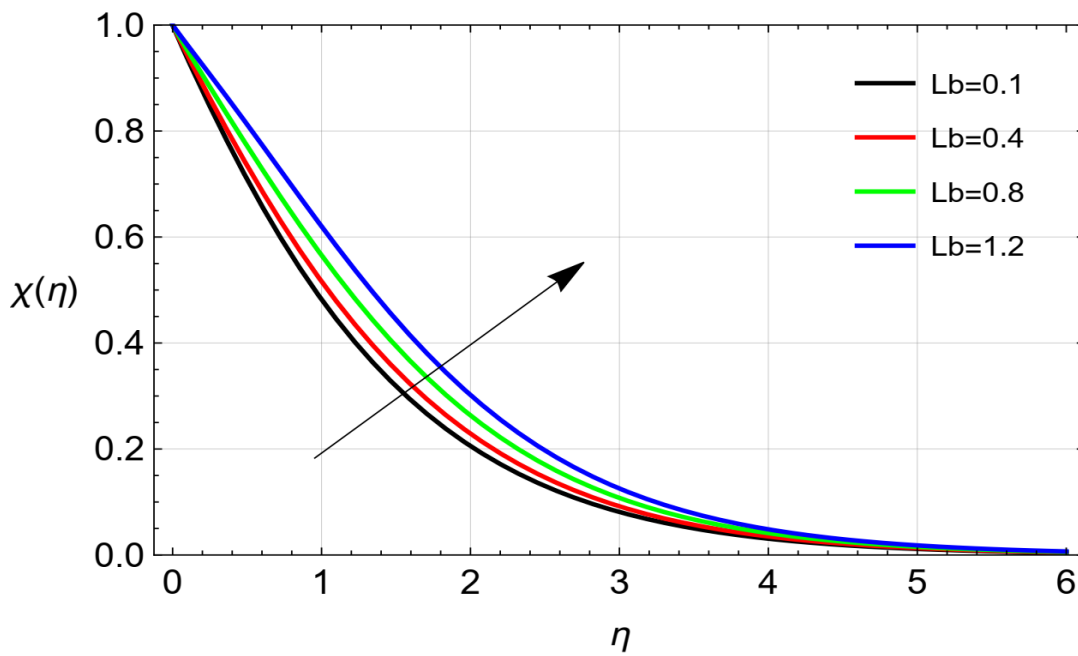


Fig. 14. Draw $\chi(\eta)$ with a rising value of L_b .

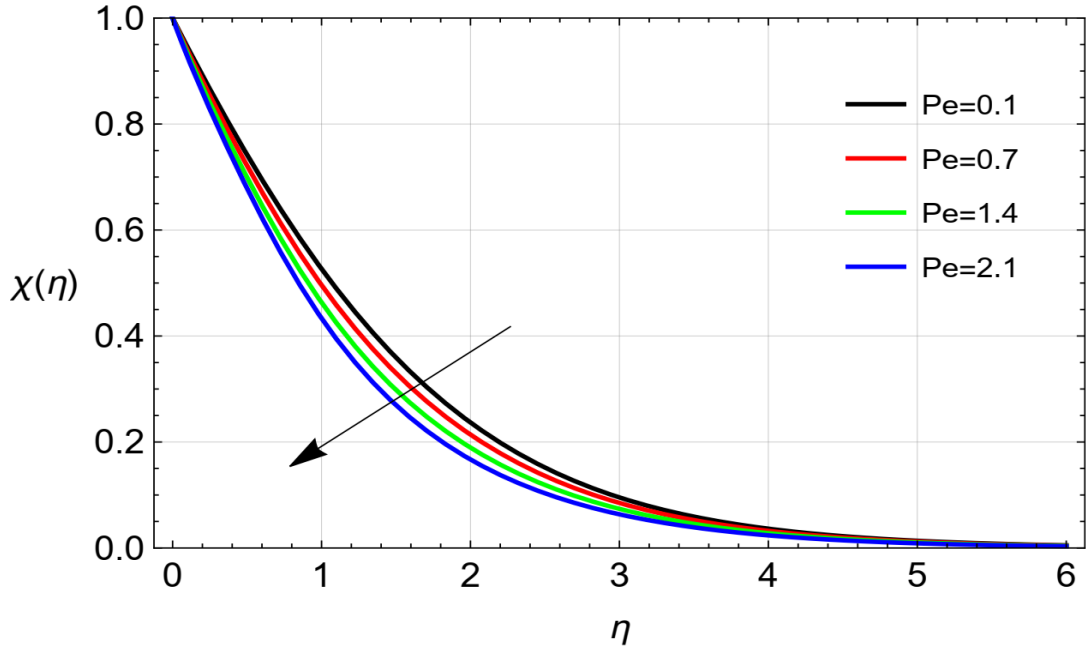


Fig. 15. Draw $\chi(\eta)$ with a varying value of Pe .

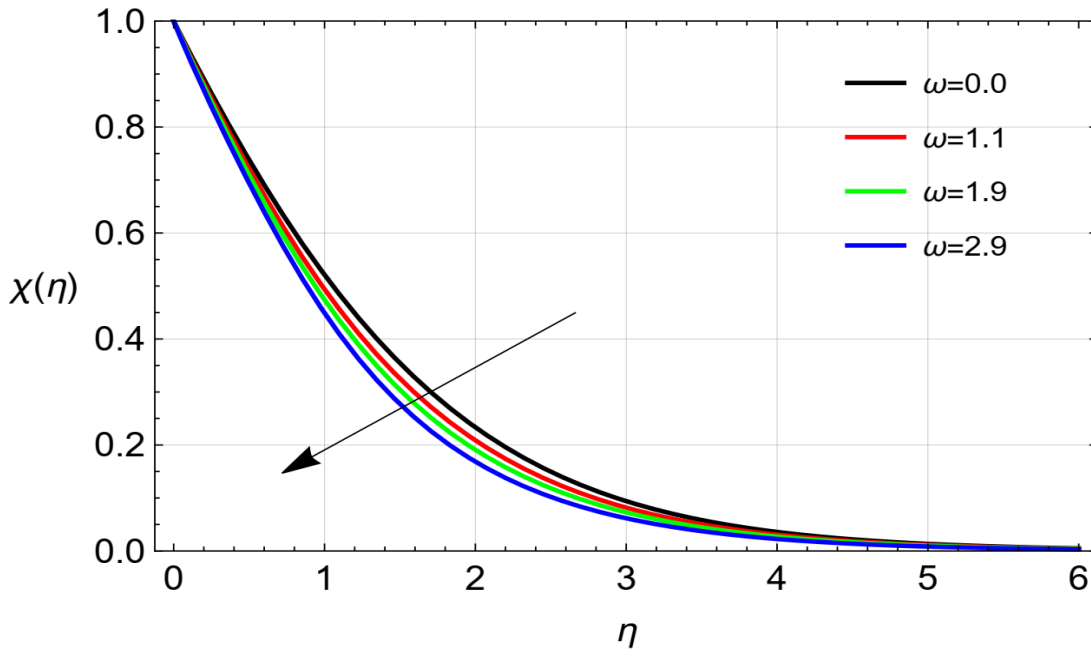


Fig. 16. Draw $\chi(\eta)$ with a varying value of ω .

Table 1. Individual average square residual errors are determined utilizing the ideal values from auxiliary parameters.

\dot{m}	$\epsilon_{\dot{m}}^f$	$\epsilon_{\dot{m}}^\theta$	$\epsilon_{\dot{m}}^\phi$	$\epsilon_{\dot{m}}^\chi$
2	2.65954×10^{-2}	7.81673×10^{-2}	6.56895×10^{-2}	1.07563×10^{-2}
6	1.78466×10^{-2}	2.6768×10^{-3}	1.05655×10^{-2}	1.55046×10^{-3}
8	9.53579×10^{-3}	1.04634×10^{-3}	9.64233×10^{-3}	5.06315×10^{-4}
14	2.74620×10^{-4}	1.00324×10^{-3}	3.95720×10^{-3}	4.59765×10^{-4}
20	1.22134×10^{-4}	9.04543×10^{-4}	1.54959×10^{-4}	4.54031×10^{-5}
24	2.60578×10^{-5}	7.75701×10^{-4}	1.40217×10^{-5}	4.58383×10^{-6}
26	1.23362×10^{-5}	2.61397×10^{-5}	1.02667×10^{-6}	2.3824×10^{-6}
28	2.40218×10^{-6}	1.42075×10^{-5}	7.91886×10^{-7}	3.16107×10^{-7}
30	3.21421×10^{-7}	1.05740×10^{-7}	4.60489×10^{-7}	6.87625×10^{-8}

Table 2. The influence of β_1, β_2 and M on skin friction when $Rd = 0.2, Pe = 0.3, N_t = 0.2, Le = 0.2, Pr = 1.0, Q = 0.2, Lb = 0.4,$ and $\omega = 0.2$.

β_1	β_2	M	$-f''(0)$
0.1	0.3	0.03	1.02202
0.2	0.3	0.03	1.03757
0.3	0.3	0.03	1.05321
0.4	0.3	0.03	1.06893
0.5	0.3	0.03	1.08473
0.01	0.1	0.03	1.08709
0.1	0.2	0.03	1.04362
0.1	0.3	0.03	1.00809
0.1	0.4	0.03	0.980489

0.01	0.5	0.03	0.96083
0.01	0.5	0.1	0.97573
0.01	0.5	0.2	0.996079
0.01	0.5	0.3	1.01533
0.01	0.5	0.4	1.03347
0.01	0.5	0.5	1.05051

Table 3. The

influence of

N_t and Q on Nusselt number, when

$M = 0.2, Lb = 0.4, \gamma = 0.3, Rd = 0.2, \omega = 0.2, F_r = 0.5, Pr = 1.0, Le = 0.2,$ and $Pe = 0.3.$

N_t	Q	$-\theta'(0)$
0.1	0.5	0.653081
0.3	0.5	0.65215
0.5	0.5	0.651224
0.7	0.5	0.650304
0.9	0.5	0.649388
0.9	0.1	0.655607
0.9	0.2	0.652499
0.9	0.5	0.649388
0.9	0.7	0.646275
0.9	0.9	0.64316

Table 4. The influence of Le, N_b and N_t on $-\phi'(0)$, when

$M = 0.2, Rd = 0.2, F_r = 0.5, Pr = 1.0, \gamma = 0.3, Pe = 0.3$ and $Q = 0.2.$

Le	N_t	N_b	$-\phi'(0)$
1.1	0.01	0.1	0.41845674
1.2	0.01	0.1	0.42655053
1.3	0.01	0.1	0.43466800
1.4	0.01	0.1	0.442809172

0.4	0.1	0.1	0.2420600
0.4	0.2	0.1	0.0434677
0.4	0.3	0.1	0.0317169
0.4	0.4	0.1	0.02123
0.4	0.3	0.2	0.18863
0.4	0.4	0.3	0.264911125
0.4	0.4	0.4	0.303065655
0.4	0.4	0.5	0.325958303

Table 5. The influence of ω and Lb on $-\chi'(0)$, when

$M = 0.2, N_t = 0.2, Rd = 0.2, F_r = 0.5, Pr = 1.0, \gamma = 0.3, Le = 0.2, Pe = 0.3$ and $Q = 0.2$.

ω	Lb	$-\chi'(0)$
0.2	0.4	0.719318
0.4	0.4	0.721581
0.6	0.4	0.723844
0.8	0.4	0.726106
0.01	0.1	0.7604
0.01	0.2	0.746122
0.01	0.3	0.731693
0.01	0.4	0.717169

Table 6. The comparison of current findings for Nusselt number.

Pr	Kandasamy et al. [47]	Sohail et al. [48]	Wang et al. [49]	Present work
0.07	0.066129	0.068735	0.0656	0.069725
0.20	0.169136	0.169892	0.1691	0.179191
0.70	0.454285	0.459843	0.4539	0.46749
2.00	0.911423	0.919975	0.9113	0.92231

7.00	1.895264	1.89674	1.8954	1.89994
20.00	3.353853	3.35708	3.3539	3.36798